Convergent close-coupling calculations of helium single ionization by antiproton impact

I. B. Abdurakhmanov,* A. S. Kadyrov, D. V. Fursa, I. Bray, and A. T. Stelbovics
ARC Centre for Antimatter-Matter Studies, Department of Applied Physics, Curtin University, Perth, WA 6152, Australia
(Received 27 October 2011; published 9 December 2011)

We apply the fully quantum-mechanical convergent close-coupling method to the calculation of antiproton scattering on the ground state of helium. The helium target is treated as a three-body Coulomb system using frozen-core and multiconfiguration approximations. The electron-electron correlation of the target is fully treated in both cases. Though both calculations yield generally good agreement with experiment for the total ionization cross sections, the multiconfiguration results are substantially higher at the lower energies than the frozen-core ones. Calculated longitudinal ejected electron and recoil-ion momentum distributions for the single ionization of helium are in good agreement with the experiment.

DOI: 10.1103/PhysRevA.84.062708 PACS number(s): 34.50.Fa, 34.10.+x

I. INTRODUCTION

Collisions of antiprotons with atoms is generally a simpler problem than for proton projectiles due to the absence of electron-capture channels. Ignoring the possibility of antiproton binding, the collision system has well-defined electronic states. The antiproton-helium collision system is a prototype of ion-atom scattering that needs to be solved before embarking on treating more complex systems. Total [1–3] and differential [4] ionization cross-section measurements exist to help in the testing of theoretical approaches to the problem.

From the theoretical point of view the antiproton-helium scattering system is a quantum-mechanical four-body problem, which cannot be solved analytically. At sufficiently high energies simple first-order perturbation methods, namely, the first Born approximation (FBA) and continuum distorted-wave eikonal initial-state (CDW-EIS) approaches, can produce reliable total ionization cross sections. At lower impact energies various nonperturbative theoretical approaches have been applied. Depending on the energy range there are some discrepancies between the various theoretical approaches, and, with experiment, it is still unclear if there is something missing in the theory that is responsible for the remaining discrepancies.

There are several approximations that may be applied to the antiproton-helium collision problem. First, the antiproton motion can be treated classically by means of straight-line trajectories. This approximation is well accepted in ion-atom collisions and its validity to reproduce correct integrated cross sections for all processes involved in antiproton-hydrogen collisions above 1 keV was recently demonstrated [5]. However, it is still unclear if this approximation is equally satisfactory for calculation of differential cross sections over a wide incident energy range. A second approximation is applied in order to avoid complications that arise from a complete description of He wave functions. Ideally, the antiproton-helium scattering must be treated as a four-body problem and the target wave functions should be obtained by diagonalizing a full three-body target Hamiltonian. The transition amplitudes in the resulting coupled equations would carry indices describing quantum states of each of the target electrons. This is far from practical even with present-day computational resources. For this reason an often-used approximation is to treat helium as a hydrogenlike target, and consequently to consider only single-ionization processes. These can be classified into two categories. The earliest ones employed the independent electron approximation in the description of He assuming that the single-electron process can be described with sufficient accuracy even without the inclusion of electron correlation effects [6–9]. More complex approaches [6,10–12] assumed the static correlation of the outer electron with the inner one constrained in the 1*s* orbital (frozen-core approximation), yielding significantly different results, especially at low energies. This by itself already clearly indicates the importance of electron correlation effects. With further advancement of computing technology new sophisticated calculations by Igarashi *et al.* [6], Pindzola *et al.* [13], Foster *et al.* [14], and Guan and Bartschat [15] became available, where multiple configurations were allowed for both target electrons. This modification improved the He wave functions and yielded an ionization potential of the ground state that is much closer to its experimental value. The resultant ionization cross sections also significantly changed from the values obtained in the frozen-core approximation. In the present work we also adopt the multiconfiguration model of the He target. The idea of including double-continuum states in the description of He structure is not feasible since in that case one runs into the problem of mixing of single- and dounble-ionization channels. This issue was addressed in Ref. [16], where the effects of double-ionization channels on the single-ionization cross section were investigated. Experimental and theoretical progress in the field of antiproton-impact-induced ionization of atoms and molecules was very recently reviewed by Kirchner and Knudsen [17].

Our goal here is to develop a fully quantum-mechanical approach to antiproton-helium collisions based on the convergent close-coupling method following the successful implementation for antiproton-hydrogen collisions [5,18]. This implies the complete relaxation of the classical limitations imposed on the relative motion of the heavy particles, i.e., the removal of the straight-line approximation mentioned above. The total scattering wave function is expanded in terms of pseudostates describing the target states of He. Those pseudostates are constructed via diagonalization of the He target Hamiltonian

*ilkhom.abdurakhmanov@postgrad.curtin.edu.au

in an orthogonal Laguerre basis assuming that one of the electrons (which is not involved in single ionization) is allowed to occupy a limited number of orbitals while the other is free to be in any other orbital necessary for convergence of the final results. When the inner electron is limited to just the $1s$ orbital of He^+ we have the frozen-core (FC) approximation, and when several inner orbitals are allowed we have the multiconfiguration (MC) description. We emphasize here that both FC and MC descriptions of the target explicitly account for the electron correlation effects. After the basis set expansion of the total wave function, the Schrödinger equation is transformed into coupled-channel Lippmann-Schwinger equations for the scattering amplitudes and solved in the impact-parameter representation. As described in Ref. [5] the impact parameter representation used in the present approach is merely a transformation from the momentum-transfer space into the mathematically equivalent impact-parameter space. The momentum-transfer and impact-parameter representations are complementary and, in principle, transform into each other without any limitation or approximation.

The plan of the paper is as follows. In Sec. II we describe our formalism for the fully quantum-mechanical treatment of the antiproton-helium collision system. The results of the frozen-core and multiconfigurational calculations as well as the relevant discussion are given in Sec. III. Finally, in Sec. IV we highlight the main results and draw conclusions from the present work. We use atomic units throughout unless otherwise specified.

II. FORMALISM

Consider scattering of an antiproton on the helium atom in its ground state. The Hamiltonian for this system is written as

$$H = H_{\rm T} - \frac{1}{2\mu}\nabla_R^2 - \frac{2}{R} + \frac{1}{|\boldsymbol{R}-\boldsymbol{r}_1|} + \frac{1}{|\boldsymbol{R}-\boldsymbol{r}_2|}, \quad (1)$$

where

$$H_{\rm T} = -\frac{1}{2}\nabla_1^2 - \frac{1}{2}\nabla_2^2 - \frac{2}{r_1} - \frac{2}{r_2} + \frac{1}{|\boldsymbol{r}_1-\boldsymbol{r}_2|} \quad (2)$$

is the target Hamiltonian, μ is the reduced mass of the projectile-target system, and $\boldsymbol{R}$, $\boldsymbol{r}_1$, and $\boldsymbol{r}_2$ denote the positions of the antiproton, electron 1, and electron 2 relative to the nucleus of helium, respectively.

The total scattering wave function Ψ for the system satisfies the Schrödinger equation

$$(H - E)\Psi(\boldsymbol{X},\boldsymbol{x}_1,\boldsymbol{x}_2) = 0, \quad (3)$$

where E is a total energy and $\boldsymbol{X}$, $\boldsymbol{x}_1$, and $\boldsymbol{x}_2$ are the coordinates of the particles including spin. Within the nonrelativistic approximation adopted in the present work, the total electronic spin of He, $\mathcal{S} = 0$, is conserved throughout the collisions, and consequently we need only to deal with $\Phi(\boldsymbol{R},\boldsymbol{r}_1,\boldsymbol{r}_2)$, the spatial part of $\Psi(\boldsymbol{X},\boldsymbol{x}_1,\boldsymbol{x}_2)$. Assuming that the possibility of antiprotonic helium formation is negligible in the energy range considered [19], we expand Φ in terms of a set of N orthogonal Laguerre-based He pseudostates ψ_i:

$$\Phi(\boldsymbol{R},\boldsymbol{r}_1,\boldsymbol{r}_2) \approx \sum_{i=1}^{N} F_i(\boldsymbol{R})\psi_i(\boldsymbol{r}_1,\boldsymbol{r}_2), \quad (4)$$

where F_i are the expansion coefficients. The index i represents a full set of quantum numbers describing the target state.

A. Helium pseudostates $\psi_i(\boldsymbol{r}_1,\boldsymbol{r}_2)$

The helium space coordinate wave functions are constructed using the configuration interaction (CI) approach of Fursa and Bray [20], namely,

$$\psi_i(\boldsymbol{r}_1,\boldsymbol{r}_2) = \sum_{\alpha,\beta} C^i_{\alpha,\beta}\phi_\alpha(r_1)\phi_\beta(r_2)\left\{Y_{l_\alpha}(\hat{r}_1)\otimes Y_{l_\beta}(\hat{r}_2)\right\}_{l_i m_i}. \quad (5)$$

Here $C^i_{\alpha,\beta}$ are the CI coefficients which are found by diagonalizing the target Hamiltonian (2). To ensure antisymmetry of the two-electron target states the following symmetry property is satisfied by CI coefficients:

$$C^i_{\alpha,\beta} = (-1)^{l_\alpha+l_\beta-l_i} C^i_{\beta,\alpha}. \quad (6)$$

Wave functions $\phi_\alpha(r)$ in Eq. (5) are the one-electron orbitals which are used to build the two-electron basis. They are made of the orthogonal Laguerre functions

$$\phi_\alpha(r) = \left(\frac{2\lambda_l(k-1)!}{(2l+1+k)!}\right)(2\lambda_l r)^{l+1}\exp(-\lambda_l r)L_{k-1}^{2l+2}(2\lambda_l r), \quad (7)$$

where $L_{k-1}^{2l+2}(2\lambda_l r)$ are the associated Laguerre polynomials with λ_l being the characteristic falloff parameter. Finally, the bipolar harmonics in Eq. (5) are defined through the spherical harmonics Y_{lm} as

$$\left\{Y_{l_\alpha}(\hat{r}_1)\otimes Y_{l_\beta}(\hat{r}_2)\right\}_{l_i m_i} = \sum_{m_\alpha m_\beta} C^{l_i m_i}_{l_\alpha m_\alpha l_\beta m_\beta} Y_{l_\alpha m_\alpha}(\hat{r}_1) Y_{l_\beta m_\beta}(\hat{r}_2),$$

where $C^{l_i m_i}_{l_\alpha m_\alpha l_\beta m_\beta}$ are Clebsch-Gordan coefficients.

Diagonalization of the target Hamiltonian $H_{\rm T}$ using the helium wave functions $\psi_i(\boldsymbol{r}_1,\boldsymbol{r}_2)$ yields negative and positive energy states ϵ_i. Presently, for the purpose of describing single ionization we restrict the upper limit of one of the indices in Eq. (5) in order to prevent the inner electron from ejecting. To be precise we include only $\{1s,2s,2p,3s,3p,3d,4s,4p,4d,4f\}$ Laguerre orbitals (7) for the description of the inner electron excitations. In order to obtain the exact He^+ $1s$ orbital and accurately take into account the short-range electron-electron correlations in the ground and low-lying energy states, the falloff parameters of the above orbitals are set equal to 2.0. The falloff parameters of the rest of the orbitals are chosen to be equal to 1.0. To maintain the orthogonality of the basis, the Gram-Schmidt orthogonalization is performed. The other index representing the one-electron states of the outer electron can be as large as required to ensure convergence of the results. In this work its upper limit is taken the same as N, i.e., the total basis size $\sum_{l=0}^{l_{\rm max}}(n_{\rm max}-l)$ with $n_{\rm max}$ and $l_{\rm max}$ being the maximum principal and orbital quantum numbers, respectively. As the basis size increases, the negative-energy states become closer to their eigenstates while the positive-energy ones provide an increasingly dense discretization of the continuum. A basis with $n_{\rm max} = 20$ and $l_{\rm max} = 5$ was sufficiently large to obtain convergent results for the cross sections presented in this work. With this basis we obtain an ionization potential of

the helium ground state of 24.544 eV, which is very close to the measured value of 24.586 eV. In order to demonstrate the effect of the inner electron excitations on the single ionization we also perform calculations assuming the FC approximation. As already mentioned, in this approximation the inner electron is always assumed to be in its $1s$ orbital; i.e., the upper limit of the index β in Eq. (5) is equal to 1. The ionization potential of the ground state in the FC approximation is 23.736 eV.

B. The coupled equations for the T matrix

Taking into account Eq. (5) we substitute expansion (4) into Eq. (3) and get a set of integro-differential equations for the expansion coefficients. Following Ref. [21] we transform them into momentum-space coupled-channel integral equations for transition matrix elements

$$T_{fi}(\boldsymbol{q}_f,\boldsymbol{q}_i) = V_{fi}(\boldsymbol{q}_f,\boldsymbol{q}_i) + \sum_{j=1}^{N}\int \frac{d\boldsymbol{q}_j}{(2\pi)^3} V_{fj}(\boldsymbol{q}_f,\boldsymbol{q}_j) G_j\left(q_j^2\right) T_{ji}(\boldsymbol{q}_j,\boldsymbol{q}_i), \tag{8}$$

where $\boldsymbol{q}_i$ is the momentum of free particle i relative to the center of mass of the bound pair in channel i. The effective two-body free Green's function in the intermediate channel j is defined as

$$G_j\left(q_j^2\right) = \left(E + i0 - \frac{q_j^2}{2\mu} - \epsilon_j\right)^{-1} \tag{9}$$

and describes the free relative motion of antiproton j and the He atom in state j with binding energy ϵ_j. The effective potentials are given by

$$\begin{aligned} V_{fi}(\boldsymbol{q}_f,\boldsymbol{q}_i) &\equiv \langle \boldsymbol{q}_f|\langle\psi_f|V|\psi_i\rangle|\boldsymbol{q}_i\rangle \\ &= \int d\boldsymbol{R} d\boldsymbol{r}_1 d\boldsymbol{r}_2 e^{-i\boldsymbol{q}_f\boldsymbol{R}} \psi_f^*(\boldsymbol{r}_1,\boldsymbol{r}_2) \\ &\quad\times \left(-\frac{2}{R} + \frac{1}{|\boldsymbol{R}-\boldsymbol{r}_1|} + \frac{1}{|\boldsymbol{R}-\boldsymbol{r}_2|}\right) e^{i\boldsymbol{q}_i\boldsymbol{R}} \psi_i(\boldsymbol{r}_1,\boldsymbol{r}_2) \\ &= \int d\boldsymbol{R} e^{i\boldsymbol{p}\boldsymbol{R}} I_{fi}(\boldsymbol{R}), \end{aligned} \tag{10}$$

where the quantity $\boldsymbol{p} = \boldsymbol{q}_i - \boldsymbol{q}_f$ is the momentum transfer. The integral $I_{fi}(\boldsymbol{R})$ in Eq. (10) is defined as

$$\begin{aligned} I_{fi}(\boldsymbol{R}) = \sum_{\alpha,\beta,\gamma,\delta,\lambda,\mu} &\sqrt{4\pi}\frac{\hat{l}_i\hat{l}_\gamma}{\hat{\lambda}} C^{(f)}_{\alpha\beta} C^{(i)}_{\gamma\delta} C^{l_f m_f}_{l_i m_i \lambda\mu} C^{l_\alpha 0}_{l_\gamma 0 \lambda 0} \\ &\times Y^*_{\lambda\mu}(\hat{\boldsymbol{R}})(-1)^{l_\alpha+l_\beta+l_i+\lambda}\langle\beta|\delta\rangle \begin{Bmatrix} l_\beta & l_\alpha & l_f \\ \lambda & l_i & l_\gamma \end{Bmatrix} \\ &\times \int_0^\infty dr_1 r_1^2 v_\lambda(R,r_1)\phi_\alpha(r_1)\phi_\gamma(r_1), \end{aligned} \tag{11}$$

where $\hat{l} = \sqrt{2l+1}$, and

$$v_\lambda(R,r_1) = 2\left(-\frac{\delta_{\lambda 0}}{R} + \frac{r_<^\lambda}{r_>^{\lambda+1}}\right). \tag{12}$$

The set of coupled integral equations in momentum space (8) is transformed into an impact-parameter representation. Details of the transformation of matrix elements into the impact-parameter space can be found in Ref. [5].

C. Ionization cross sections

The total ionization cross sections can be obtained from the integrated cross sections for the transitions to the open positive-energy states. The integrated cross sections for any transition σ_{fi} are directly related to the transition matrix elements T_{fi}:

$$\sigma_{fi} = \frac{\mu^2}{4\pi^2}\frac{q_f}{q_i}\int |T_{fi}(\boldsymbol{q}_f,\boldsymbol{q}_i)|^2 d\Omega_{\boldsymbol{q}_f}, \tag{13}$$

where $\Omega_{\boldsymbol{q}_f}$ represents the angular variables of the scattered antiproton.

As far as the differential ionization is concerned, various differential cross sections can be obtained using the ionization amplitude. In our previous paper on differential ionization of atomic hydrogen by antiproton impact [18], we described how to generate the ionization amplitude from the transition matrix elements T_{fi}. The same technique can be applied here as well, provided He is considered in the FC approximation, i.e., the inner electron is always in its $1s$ orbital. Thus, in the frozen-core approximation the ionization amplitude corresponding to the ejected electron momentum κ can be written as

$$T^N_{\boldsymbol{\kappa}}(\boldsymbol{q}_f,\boldsymbol{q}_i) = \sum_{l_f=0}^{l_{\max}}\sum_{m_f=-l_f}^{l_f} F_{l_f m_f}(\boldsymbol{q}_f,\boldsymbol{q}_i,\kappa) Y_{l_f m_f}(\hat{\boldsymbol{\kappa}}), \tag{14}$$

where $F_{l_f m_f}(\boldsymbol{q}_f,\boldsymbol{q}_i,\kappa)$ is a function generated as a result of an interpolation of $\sqrt{2/\pi}(-i)^{l_f} e^{i\sigma_{l_f}} f_{n_f l_f}(\kappa) T_{fi}(\boldsymbol{q}_f,\boldsymbol{q}_i)$ on a grid of the ejected electron energies. Here $\{n_f l_f m_f\}$ represents the full set of quantum numbers of the final state f and σ_{l_f} is the Coulomb phase shift of He in the static exchange approximation. The function $f_{n_f l_f}(\kappa_{n_f l_f})$ in this case is constructed from overlaps between the radial Coulomb wave U_{l_f} and the one-electron orbitals $\phi_{n_f l_f}$:

$$\begin{aligned} f_{n_f l_f}(\kappa) = \langle\phi_{1s}|\phi_{1s}\rangle &\int_0^\infty U_{l_f}(\kappa,r)\phi_{n_f l_f}(r) r^2 dr \\ &+ \langle\phi_{1s}|\phi_{n_f l_f}\rangle \int_0^\infty U_{l_f}(\kappa,r)\phi_{1s}(r) r^2 dr. \end{aligned} \tag{15}$$

Once the ionization amplitude is obtained we can immediately relate it to the fully differential ionization cross section as

$$\frac{d^3\sigma(\boldsymbol{q}_f,\boldsymbol{q}_i,\boldsymbol{\kappa})}{dE d\Omega_e d\Omega_p} = \mu^2 \frac{q_f \kappa}{q_i} |T_{\boldsymbol{\kappa}}(\boldsymbol{q}_f,\boldsymbol{q}_i)|^2. \tag{16}$$

By sequentially integrating the fully differential ionization cross section over angular variables of the scattered antiproton and the ejected electron we can find various double- and single-differential-ionization cross sections. Such quantities presently lack experimental investigation. Carrying out such kinematically complete experiments is currently problematic due to the difficulties related to the production of a stable high-intensity antiproton beam. However, the recent development of recoil-ion and ejected-electron-momentum spectroscopy makes accurate measurements of differential cross sections in the momenta of these particles possible. In fact, the recoil ion carries as much information on the three-body ionization

dynamics as the projectile and the ejected electron. Such a pioneering experiment [4] on antiproton impact ionization of He was already reported at 945 keV, which tabulates the single-differential cross section as a functions of the longitudinal recoil-ion and the ejected-electron momenta. These quantities can be obtained from the double-differential-ionization cross section $d^2\sigma(q_f,q_i,\kappa)/dEd\Omega_e$ if we employ the following dynamic constraints required by the energy and momentum conservation:

$$p_{r\parallel} = p_\parallel - \kappa_\parallel = \frac{\epsilon_f - \epsilon_0}{v} - \kappa\cos\theta_e, \tag{17}$$

where $p_{r\parallel}$ and $\kappa_\parallel$ are, respectively, the longitudinal momenta for the recoil ion and the ionized electron, and $p_\parallel$ is the longitudinal projectile momentum transfer. With this we can write

$$\frac{d\sigma}{d\kappa_\parallel} = \int_{\kappa_\parallel^2/2}^{\infty} \frac{1}{\kappa}\frac{d^2\sigma}{dEd\Omega_e}dE \tag{18}$$

and

$$\frac{d\sigma}{dp_{r\parallel}} = \int_{\epsilon^-}^{\epsilon^+} \frac{1}{\kappa}\frac{d^2\sigma}{dEd\Omega_e}dE. \tag{19}$$

The integration limits of Eq. (19) can be obtained from Eq. (17) or

$$\kappa^\pm = v\cos\theta_e \pm \sqrt{v^2\cos^2\theta_e + 2(p_{r\parallel}v - |\epsilon_0|)} \tag{20}$$

with $\epsilon^\pm = (\kappa^\pm)^2/2$.

III. RESULTS AND DISCUSSION

Here we present our numerical results for the grand total as well as various differential single-ionization cross sections. Figure 1 shows the total cross section for the single ionization of helium under the impact of an antiproton with the incident energy ranging from 1 keV to 1 MeV. Experimentally this process was studied on three occasions. Most recently the group at CERN [1] conducted an experiment with antiproton impact energies as low as 3.42 keV. These measurements exhibit a quite slow fall of the cross section with the decreasing impact energy. Two points of this data set at energies ≈20 and 25 keV reasonably overlap with the earlier experiment by Hvelplund *et al.* [3], which in turn is in overall agreement with the oldest experiment by Andersen *et al.* [2]. The model curves represent our frozen-core convergent close-coupling (CCC) results as well as the results of semiclassical calculations by Igarashi *et al.* [6], McGovern *et al.* [10], and Lee *et al.* [11] utilizing a similar treatment of the target. Here we refer to the presented calculations with the single acronym FC, since they all start off by diagonalizing the helium Hamiltonian in a suitable two-electron basis with the assumption that the inner electron is always in the ground state. The only difference is that different representations of the radial part of the target wave function are used: Slater-type orbitals (STOs) by Lee *et al.* [11], Sturmian functions by Igarashi *et al.* [6], and Laguerre functions by McGovern *et al.* [10] and the present fully quantum-mechanical model. The crosses show the one-active-electron (OAE) calculations of Pindzola *et al.* [13] with the Hartree local exchange potential. These results are considerably larger than the other FC calculations as well as the experiments. They concluded that the electron-correlation effects of the target, not included in the OAE calculations, play a significant role. The other calculations are in quite good agreement with each other and the experiment over most of the energy range. We next turn to MC results.

Figure 2 compares the experimental data with the calculations which allow multiple configurations for the core electron. Thus the current approach and that of Igarashi *et al.* [6] includes double-excitation and single-ionization channels. Whereas we allow the inner electron to take all excited states with maximum principal quantum number $n_{\max} \leqslant 4$, Igarashi *et al.* [6] limited the number of excited core states

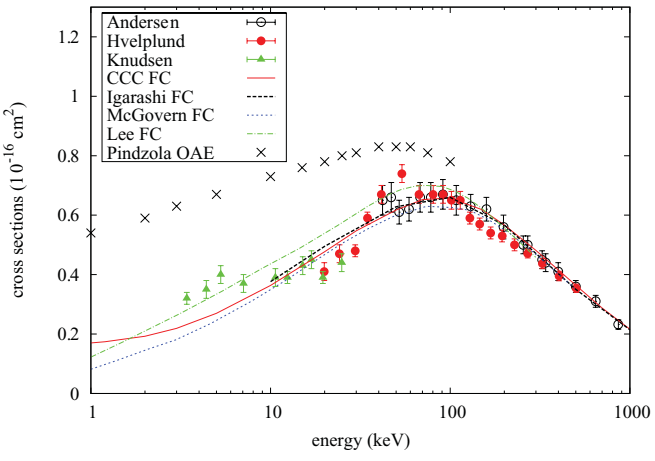

FIG. 1. (Color online) Total single-ionization cross section for antiproton-helium scattering. Experimental data by Knudsen *et al.* [1] (▲), Hvelplund *et al.* [3] (•), and Andersen *et al.* [2] (○). Various frozen-core (FC) semiclassical close-coupling calculations are due to Igarashi *et al.* [6], McGovern *et al.* [10], and Lee *et al.* [11]. The one-active-electron semiclassical close-coupling calculations are due to Pindzola *et al.* [13]. The present frozen-core calculations are denoted by CCC FC.

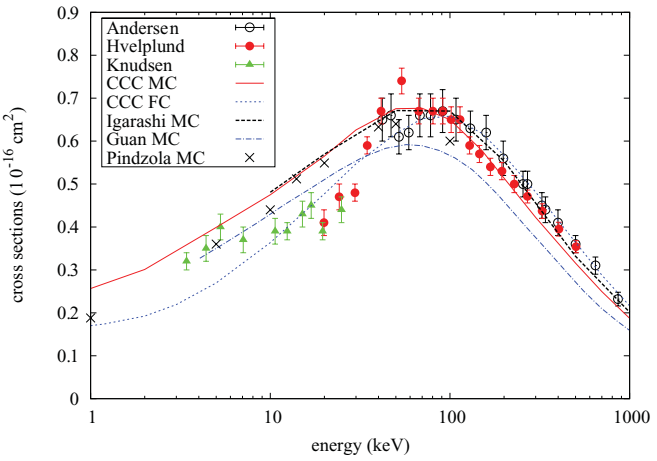

FIG. 2. (Color online) Total single-ionization cross section for antiproton-helium scattering. Experimental data by Knudsen *et al.* [1] (▲), Hvelplund *et al.* [3] (•), and Andersen *et al.* [2] (○). Various multiconfigurational (MC) semiclassical close-coupling calculations are due to Igarashi *et al.* [6], Guan and Bartschat [15], and Pindzola *et al.* [13]. The present multiconfigurational calculations are denoted by CCC MC. The CCC FC results are also presented.

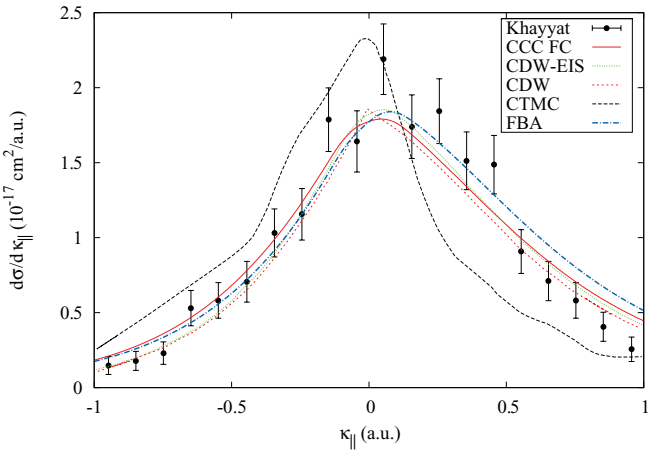

FIG. 3. (Color online) Ejected-electron longitudinal momentum distribution for single ionization of helium by 945-keV antiproton impact. Experimental data (•) and CDW and CTMC calculations are due to Khayyat *et al.* [4]. CDW-EIS calculations are due to Fainstein and Rodriguez [23]. The present frozen-core calculations are denoted by CCC FC. First Born results are also shown.

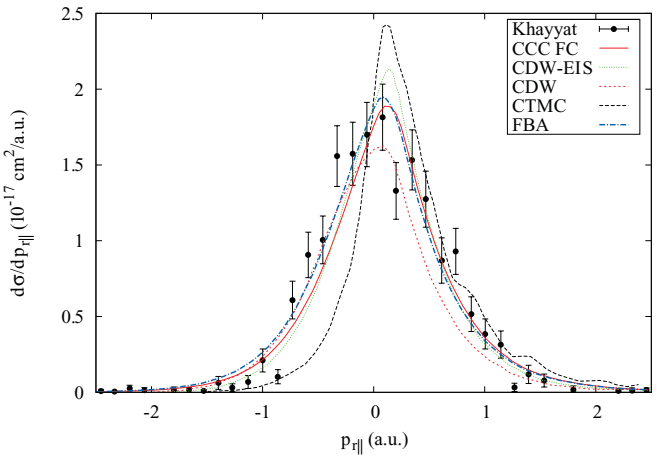

FIG. 4. (Color online) Recoil-ion longitudinal momentum distribution for single ionization of helium by 945-keV antiproton impact. Experimental data (•) and CDW and CTMC calculations are due to Khayyat *et al.* [4]. CDW-EIS calculations are due to Fainstein and Rodriguez [23]. The present frozen-core calculations are denoted by CCC FC. First Born results are also shown.

to $n_{\max} = 3$. In addition to the discrete doubly excited states, the calculations by Foster *et al.* [14], Guan and Bartschat [15], and Pindzola *et al.* [13] also include double-ionization states. Apart from the results of Guan and Bartschat [15], which are systematically lower, there is good agreement between the various MC calculations over the entire energy range. What is particularly interesting is the comparison with the FC results, only given for the CCC theory. At energies above 100 keV the MC results are a little lower than the FC ones. However, at lower energies the MC results are substantially larger. Following a similar study for electron scattering [22], we might have expected that an increase in the ionization threshold would result in a systematic drop of the total ionization cross section. Perhaps this is still the case at energies above 100 keV, but we are unable to find a definitive argument why the MC-calculated cross sections should be above the FC ones at low energies. We do note that, unlike in the electron projectile case, the velocity of the antiproton near the ionization threshold is much lower than the orbiting electron. Consequently the comparison of the two projectiles is more appropriate at higher energies than near threshold.

Figure 3 shows the ejected-electron longitudinal momentum distribution in single ionization of helium by antiproton impact at 945 keV. We compare our FC results with the experimental data of Khayyat *et al.* [4] and other calculations. Apart from the classical-trajectory Monte Carlo (CTMC) calculations, there is good agreement between the various theories and experiment. The CCC results are only a marginal improvement on the Born approximation due to the relatively high energy being considered.

The corresponding recoil-ion longitudinal momentum distribution is given in Fig. 4. Once more only the CTMC approach clearly fails to describe the experiment. Perhaps the CDW results show a systematic discrepancy at the positive momentum values. The considered impact energy is so large that even the simplest FBA is not significantly different from the present results and other more sophisticated perturbation methods. Similar measurements, but at lower impact energies, would be very helpful in testing the newly developed CCC approach to antiproton-impact fully differential ionization. To demonstrate how the Born and CCC results differ at lower energies, in Fig. 5 we present He single ionization by antiproton impact at energies of 100 and 300 keV. In line with our expectations the differences between the CCC FC and the first Born distributions increase as the impact energy decreases. Interestingly, as we go down in the impact energy the curves are developing a two-maxima structure which is more pronounced at lower energies. We note that the magnitude of the longitudinal momentum distribution gets larger with decreasing incident energy.

Finally we report that, in addition to the longitudinal momentum distributions, by carrying out a fully

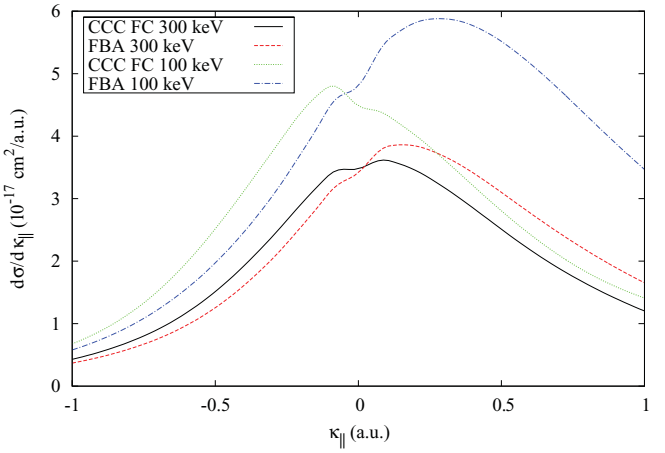

FIG. 5. (Color online) Ejected-electron longitudinal momentum distribution for single ionization of helium by antiproton impact at various incident energies. Relevant first Born results are also presented for comparison.

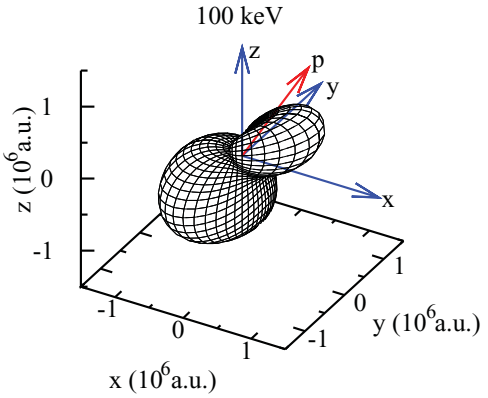

FIG. 6. (Color online) Three-dimensional plot of the triply differential cross section for antiproton-impact single ionization of helium at 100 keV. The scattering plane is defined by $\boldsymbol{p} = 0.6$ a.u. and the ejection energy of the electron is 5 eV. The arrow is pointing in the direction of the momentum transfer.

quantum-mechanical CCC approach we can give any differential cross section for the single ionization of He by antiproton impact. This was shown recently in the case of antiproton-hydrogen scattering [18]. In the present work we limit our illustrative demonstration by giving in Fig. 6 the three-dimensional distribution of the fully differential cross section for the 100-keV antiproton-impact single ionization of He with the ejected-electron energy of 5 eV and a momentum transfer of $\boldsymbol{p} = 0.6$ a.u. In this figure the antiproton is incident in the z direction and scattered in the negative x direction. Whereas the Born approach (not shown) produces the rotationally symmetric angular distribution of the ejected electrons around the momentum transfer $\boldsymbol{p}$, in the CCC FC approach, this distribution strongly deviates from the rotational symmetry. At this impact energy the postcollision interaction becomes significant. Due to the strong repulsion of the ejected electron from the scattered antiproton, the binary peak is smaller than the recoil peak. Other differential cross sections can be provided upon request.

IV. CONCLUSION

We applied the fully quantum-mechanical convergent close-coupling method to the calculation of antiproton scattering on the ground state of He. The target is treated as a three-body Coulomb system, with the inner electron being either frozen into the He^+ 1s orbital (frozen-core approximation) or allowed to be described by a limited number of negative-energy orbitals (multiconfiguration approximation). Consequently, the electron-electron correlation of the target is fully treated in both cases. It is found that the multiconfigurational treatment of the target yields significantly higher total ionization cross sections at lower impact energies than does the frozen-core treatment. Agreement with the total ionization cross-section measurements is satisfactory over most of the energy range, with the lower energies inviting more investigation. The frozen-core approach allows us to calculate fully differential, as well as all other differential, single-ionization cross sections. Calculated longitudinal ejected-electron and recoil-ion momentum distributions for the single ionization of helium are in good agreement with the experiment.

ACKNOWLEDGMENTS

The work was supported by the Australian Research Council. We are grateful for access to the Australian National Computing Infrastructure Facility and its Western Australian node iVEC. We thank Professor M. S. Pindzola for sending his results in a tabulated form.

[1] H. Knudsen *et al.*, Phys. Rev. Lett. **101**, 043201 (2008).
[2] L. H. Andersen, P. Hvelplund, H. Knudsen, S. P. Møller, J. O. P. Pedersen, S. Tang-Petersen, E. Uggerhøj, K. Elsener, and E. Morenzoni, Phys. Rev. A **41**, 6536 (1990).
[3] P. Hvelplund, H. Knudsen, U. Mikkelsen, E. Morenzoni, S. P. Møller, E. Uggerhøj, and T. Worm, J. Phys. B **27**, 925 (1994).
[4] K. Khayyat *et al.*, J. Phys. B **32**, L73 (1999).
[5] I. B. Abdurakhmanov, A. S. Kadyrov, I. Bray, and A. T. Stelbovics, J. Phys. B **44**, 075204 (2011).
[6] A. Igarashi, A. Ohsaki, and S. Nakazaki, Phys. Rev. A **62**, 052722 (2000).
[7] G. Schiwietz, U. Wille, R. D. Muio, P. D. Fainstein, and P. L. Grande, J. Phys. B **29**, 307 (1996).
[8] L. A. Wehrman, A. L. Ford, and J. F. Reading, J. Phys. B **29**, 5831 (1996).
[9] S. Sahoo, S. Mukherjee, and H. Walters, Nucl. Instrum. Methods **233**, 318 (2005).
[10] M. McGovern, D. Assafrão, J. R. Mohallem, C. T. Whelan, and H. R. J. Walters, Phys. Rev. A **79**, 042707 (2009).
[11] T. G. Lee, H. C. Tseng, and C. D. Lin, Phys. Rev. A **61**, 062713 (2000).
[12] F. Martin and A. Salin, Phys. Rev. A **54**, 3990 (1996).
[13] M. S. Pindzola, T. G. Lee, and J. Colgan, J. Phys. B **44**, 205204 (2011).
[14] M. Foster, J. Colgan, and M. S. Pindzola, Phys. Rev. Lett. **100**, 033201 (2008).
[15] X. Guan and K. Bartschat, Phys. Rev. Lett. **103**, 213201 (2009).
[16] A. Igarashi, A. Ohsaki, and S. Nakazaki, Phys. Rev. A **64**, 042717 (2001).
[17] T. Kirchner and H. Knudsen, J. Phys. B **44**, 122001 (2011).
[18] I. B. Abdurakhmanov, A. S. Kadyrov, I. Bray, and A. T. Stelbovics, J. Phys. B **44**, 165203 (2011).
[19] R. Ahlrichs, O. Dumbrajs, H. Pilkuhn, and H. G. Schlaile, Z. Phys. A **306**, 297 (1982).
[20] D. V. Fursa and I. Bray, Phys. Rev. A **52**, 1279 (1995).
[21] I. H. Sloan and E. J. Moore, J. Phys. B: At. Mol. Phys. **1**, 414 (1968).
[22] I. Bray and D. V. Fursa, J. Phys. B **44**, 061001 (2011).
[23] P. D. Fainstein and V. D. Rodriguez, J. Phys. B **33**, 4637 (2000).